

RESEARCH ARTICLE

Using the daily change in the Southern Oscillation Index to develop analogues and the relationship to severe weather outbreaks

Joseph S. Renken¹ | Caleb L. Brown^{2,3} | Grace Kennedy³ | Jacques Mainguy⁴ |
Nicholas Wergelas⁵ | Anthony R. Lupo³ 

¹Organic Forecasting, LLC, Columbia, Missouri, USA

²National Weather Service, North Platte, Nebraska, USA

³Atmospheric Science Program, School of Natural Resources, University of Missouri, Columbia, Missouri, USA

⁴System Data Experts, Calgary, Alberta, Canada

⁵Department of Electrical Engineering and Computer Science, University of Missouri, Columbia, Missouri, USA

Correspondence

Anthony R. Lupo, Atmospheric Science Program, School of Natural Resources, University of Missouri, Columbia, MO 65211, USA.

Email: lupoa@missouri.edu

Abstract

The occurrence of severe weather is an annual problem for much of the United States and North America and maximizes from March through June. With the increased interest in subseasonal weather forecasting, there have been attempts to anticipate the occurrence of anomalous weather on the time-scale of one to 4 weeks including the occurrence of severe weather. Previous research has shown that teleconnection indices, associated with long period Rossby wave activity, or persistent large-scale flow regimes have been useful tools in this endeavour. Here, abrupt changes over a 24–72-hr period (10 or more units per day or 20 or more units over 3 days) in the Southern Oscillation Index (SOI) time series will be used to demonstrate that these changes can be associated with the possible occurrence of major severe weather event-days defined as; 20 or more tornado, 155 or more wind speed events $>25.9 \text{ m}\cdot\text{s}^{-1}$, or 135 or more hail diameter larger than 25.4 mm, reports over the United States one to 3 weeks in advance, especially during the March through June period. The severe weather events obtained from the archive at the Storm Prediction Center (SPC) from 1991 through 2020 were used. The results here demonstrate that more than 7 in 10 major severe weather occurrences were associated with abrupt positive and negative changes in the daily SOI when using signal detection methods.

KEYWORDS

ENSO, interannual variability, severe weather, Southern Oscillation Index, subseasonal

1 | INTRODUCTION

Subseasonal phenomena (e.g., Weickmann and Berry, 2009; Robertson *et al.*, 2015) and forecasting have been topics of great interest during the last several years. Previous research (e.g., Renken *et al.*, 2017) demonstrated that there is detectable variability on the one-to-four-week timescale in the 500 hPa height field when decomposing the

climatological time series of the Pacific North American (PNA) Index to wave space using Fourier transforms. They identified 7–11, 17, 21 and 24-day cycles in the index using Fourier decomposition of the index from 1950 to 2017, and this appears to support early work such as Branstator (1987) who found similar periodicity (16–23 days) in the upper troposphere and stratosphere during the winter of 1979–1980 using empirical orthogonal function (EOF)

analysis. Renken *et al.* (2017) demonstrated also the utility of the Bering Sea Rule (BSR) and East Asia Rule (EAR) Indices in skilfully projecting unusual (two standard deviation or greater) warm or cool periods for the central United States using analogues and this predictability is likely due to long period Rossby wave propagation (e.g., Zhao *et al.*, 2010; Farrar, 2011; Wang *et al.*, 2013; Seo *et al.*, 2016). These studies have identified periodic fluctuations of the PNA index in the Pacific and North America region due to these Rossby waves up to almost 40 days.

Renken *et al.* (2017) and Nunes *et al.* (2017) also demonstrated the linkage of blocking anticyclones to excessively cold periods over the middle of the United States. Renken *et al.* (2017) also suggested that severe weather outbreaks may be anticipated using these techniques. Previously, it was considered that predictability beyond the well-known forecast wall (e.g., 10–14 days; Jensen *et al.*, 2018) is not possible using dynamic techniques based on the primitive equations (e.g., Li, 2018) although skilful prediction of changes in the large-scale flow regime out to 10 days or beyond using ensemble models, statistical techniques, or a blend of these is increasing the forecast horizon (e.g., Klaus *et al.*, 2020, and references therein). Additionally, Gensini and Tippett (2019) show skill in ensemble model forecasts for tornado day events out to 9 days and at Day 12 for hail events.

Baggett *et al.* (2018) show skilful forecasts of severe weather at the subseasonal timescale (2–5 weeks) associated with the MJO. Then, Gensini *et al.* (2019) demonstrate the link between tropical convection associated with a half-MJO cycle (from the Indian Ocean to Central Pacific) 20–30 days in advance (about 27 days) with the active late May tornado outbreak in 2019. Also, Miller *et al.* (2020) use a hybrid statistical–dynamic technique to project tornado outbreak frequency out to week three with skill better than climatology. Their paper examined the association of severe weather with persistent weather regimes during May, which is the peak month for the occurrence of tornadoes. They found one particular regime (anomalously low heights over the northwest United States and higher heights over the southeast United States) was associated with at least one tornado occurrence more than 70% of the time. Additionally, they also found that the results were equally valid for March and April as well.

Intraseasonal variability and the link to severe weather outbreaks in the United States has been shown previously (Barrett and Gensini, 2013; Thompson and Roundy, 2013; Barrett and Henley, 2015; Bosart *et al.*, 2017; Tippett, 2018). Thompson and Roundy (2013) demonstrated that extreme (or violent) spring season severe weather outbreaks (1974–2010) are more likely during phase 2 of the Real-time Multivariate (RMM) index phase of the Madden–Julian Oscillation (MJO) also known as the Intraseasonal

Oscillation (ISO). This result is confirmed by Moore and McGuire (2020) for the spring. Barrett and Gensini (2013) found that all tornado days (1990–2011) in April (May) are more likely during MJO phase 6 and 8 (phase 5 and 8), and less likely during phases 3, 4, and 7 (phases 2 and 3). These results seem to contradict Thompson and Roundy (2013), but each examined different datasets. Barrett and Henley (2015) find a positive relationship between MJO phase 2 and hail days during April similar to Thompson and Roundy (2013). Bosart *et al.* (2017) demonstrated a tropical to mid-latitude connection to extreme weather over North America via the propagation of Rossby wave trains (RWT). Much of the work cited in the previous two paragraphs formed the basis for the creation of the Extend-Range Tornado Activity Forecast (ERTAF) project (see Gensini *et al.*, 2020).

Many others have demonstrated that there is inter-annual variability in the occurrence of severe spring season weather as associated with the El Niño–Southern Oscillation (ENSO) (e.g., Akyuz *et al.*, 2004, and references therein). Monfredo (1999), Cook and Schaefer (2008), and Moore *et al.* (2018) also demonstrate a link between the phase of ENSO and the occurrence of tornadoes in the United States. Monfredo (1999) and Moore *et al.* (2018) find that the La Niña phase favoured higher tornado numbers in the continental United States (CONUS) during the severe weather season as defined by each respective work. Akyuz *et al.* (2004) showed that there was a slight preference for La Niña years, but that the spatial variations of where tornadoes occur preferentially in relation to ENSO. This result confirmed those of Marzban and Schaefer (2001) and then echoed later by Cook and Schaefer (2008), although the latter also found ENSO neutral years favoured more tornado occurrences. Allen *et al.* (2015) demonstrated that La Niña years favoured the occurrence of tornado and hail events over El Niño across the United States. Cook *et al.* (2017) found that the southeastern United States (e.g., Dixon *et al.*, 2011) was more active (from 1950 to 2016) during La Niña years while the southern and central plains region of the United States was more active during El Niño years. Moore (2019) shows that ENSO variability in the USA is a function of season. Lepore *et al.* (2017) demonstrate that winter season ENSO phase can be used to anticipate spring season severe weather (tornado and hail) activity. Their work implied that La Niña years showed more success, especially for hail events.

Additionally, the El Niño phenomenon in South America was linked to the long-term (monthly) behaviour of the Southern Oscillation Index (SOI is the difference between the pressure at sea level for Tahiti minus Darwin) by Bjerknes (1966, 1969). It is well known that ENSO influences the primary location of equatorial

region convection as well as the strength and location of the Walker circulation. Tropical convection in turn has been shown by many researchers to influence the strength and phase of mid-latitude low frequency circulation through the propagation of Rossby and Kelvin waves (e.g., Wallace and Gutzler, 1981; Renwick and Revell, 1999 or MJO see Pan and Li, 2008; Henderson *et al.*, 2016; Gollan and Greatbatch, 2017) in both hemispheres. Since the monthly and daily SOI index has been used to define the phase of ENSO, it may be possible to use abrupt changes in the daily SOI to change in the mid-latitude weather over North America that may accompany severe weather.

The goals of this work are as follows: (a) to demonstrate that there is subseasonal variability in the daily Southern Oscillation Index (dSOI) and the time derivative from 1991 to 2020, (b) this information as well as the results of Renken *et al.* (2017) can be used to detect outbreaks of different modes of severe weather, and (c) that the ability of dSOI to detect severe weather may vary interannually (and in particular with ENSO). The utilization of the time rate of change of teleconnection indices has precedent. Gensini and Marinaro (2016) and Gensini and Allen (2018) use the global relative angular momentum (Global Wind Oscillation [GWO]) and the time derivative, demonstrating that the low angular momentum state is related to increased tornado and hail frequencies in the United States. Lupo *et al.* (2014), Newberry *et al.* (2016), and Henson *et al.* (2017) use the ENSO and seasonal change in ENSO phase as related to summer season North American weather as well as that in Eastern Europe or Western Russia. The latter examined the seasonal transition in ENSO phase and related this transition to agricultural yields. Thus, the results of these study objectives proposed above would provide a forecaster another tool for anticipating severe weather beyond 1 week. Section 2 describes the data and methods used here. Section 3 analyses the dSOI time series, and section 4 examines the major severe weather events identified for this study and the ability of the dSOI index and the daily change in SOI to correlate with the occurrence of severe weather events as in Renken *et al.* (2017).

2 | DATA AND METHODS

2.1 | Data

The data used for this research can be found at several sources, including the National Centers for Environmental Prediction/National Centers for Atmospheric Research (NCEP/NCAR) reanalyses (Kalnay *et al.*, 1996). We also used the National Centers for Environmental Information (NCEI)

climatic information (teleconnections and climatological information such as surface temperatures). The NCEP/NCAR reanalysis data used were the 500 hPa height fields on a $2.5^\circ \times 2.5^\circ$ latitude/longitude grid four times daily from 1948 to the present. The SOI index information was available through the Bureau of Meteorology (BOM) (Australia) website (<https://data.longpaddock.qld.gov.au/SeasonalClimateOutlook/SouthernOscillationIndex/SOIDataFiles/DailySOI1887-1989Base.txt>) from June 6, 1991 to December 31, 2020. The period from January 1, 1991 to June 5, 1991 was obtained by using daily pressure data obtained for Tahiti and Darwin and then SOI was calculated using the BOM formulation,

$$SOI = 10 \frac{Pd_{diff} - \overline{Pd_{diff}}}{SD(Pd_{diff})}. \quad (1)$$

In Equation (1), Pd_{diff} is the sea level pressure difference between Tahiti and Darwin, and $\overline{Pd_{diff}}$ is the long-term monthly average of the quantity, whereas $SD(Pd_{diff})$ is the long-term standard deviation. This provides for a complete 30-year period. The severe weather storm reports (January 1, 1991 to December 31, 2020) can be found at two sites (<https://www.spc.noaa.gov> and <https://www.ncdc.noaa.gov/stormevents/>). The filtered counts of severe weather occurrence were used from the Severe Storms Prediction Center (SPC) archive.

2.2 | Methods

The 24- and 72-hr change in daily SOI (defined as dSOI here in order to differentiate from the monthly value) was calculated from January 1, 1991 to December 31, 2020 (10,958 points). The 24- and 72-hr change in dSOI was calculated respectively as

$$(dSOI_{day+1} - dSOI_{day}), \quad (2a)$$

$$(dSOI_{day+3} - dSOI_{day}). \quad (2b)$$

Then a Fourier transform was applied to each time series and the result plotted in wave space. In order to test for significant periods (e.g., Newberry *et al.*, 2016; Renken *et al.*, 2017), a statistical test assuming a white noise spectrum a priori was applied following Wilks (2006) and testing at the 95% confidence level ($p = .05$). Then, a dSOI change event was counted as a time period when one or several consecutive days recorded a dSOI change of the same sign. This resulted in 1,708 10-point change events and 1,129 20-point change dSOI events

TABLE 1 List of ENSO years used here

El Niño (EN)	Neutral (NEU)	La Niña (LN)
1991	1990	1998–1999
1997	1992–1996	2007
2002	2000–2001	2010
2006	2003–2005	2017
2009	2008	2020
2014–2015	2011–2013	
2018	2016	
	2019	

Note: The years below are taken from the Center for Ocean and Atmosphere Prediction Studies (<http://www.coaps.fsu.edu>).

over the entire 30-year period. The values 10 and 20 were used to identify a change in dSOI event since these values are larger than one and two standard deviations in dSOI change, respectively (see section 3).

In order to examine the occurrence of severe weather and produce a large enough sample size for each mode (tornado, hail diameter ≥ 25.4 mm, and wind speeds ≥ 25.9 m·s⁻¹), a major severe weather event (day) was defined here subjectively as a day with the number of reports over the entire United States as follows:

- 20 or more tornadoes.
- 155 or more wind speeds ≥ 25.9 m·s⁻¹.
- 135 or more hail diameter ≥ 25.4 mm.

This produced 358 tornado days, 365 wind event days, and 309 hail event days, and these days were not always mutually exclusive. However, we do study these events as independent time series as several references in the introduction have done, and then a subset of these days where all three criteria are met on the same day. Then the annual temporal distributions of severe weather occurrence were plotted and the synoptic-scale environment of these events were examined. The distributions of the severe weather occurrences were tested using the chi-square goodness-of-fit test (e.g., Wilks, 2006).

The dSOI information and severe weather were then stratified by ENSO phase. The definition for ENSO used here is described in, for example, Newberry *et al.* (2016), Henson *et al.* (2017), or Lupo *et al.* (2019), and references therein, and a short description is given here. The Japanese Meteorological Agency (JMA) ENSO index is available through the Center for Ocean and Atmospheric Prediction Studies (COAPS) from 1868 to present (<https://www.coaps.fsu.edu>). The JMA classifies ENSO phases using SST within the bounded region of 4°S–4°N,

150°–90°W, and defines the commencement of an ENSO year as 1 October, and its conclusion on 30 September of the next year. This index is widely used in other published works (see Newberry *et al.*, 2016 and references therein), and a list of years is given in Table 1. Finally, the ability of the dSOI change index to detect the occurrence of severe weather is examined.

Signal detection theory was used here to evaluate the utility of the dSOI as a forecast tool. This is typically used in short range forecasting, such as the occurrence of severe weather (e.g., Brooks, 2004), but Renken *et al.* (2017) used this for subseasonal range forecasting. It is based on a contingency table for weather events forecast and observed (Table 2). From signal detection theory, X is the number of severe weather occurrences that were associated with dSOI change events and represents a correct forecast, and Y is the number of severe weather events that occurred and no dSOI change events were associated with it. The value Z is the number of dSOI change events that occurred without a severe weather event, and W is the number of days with no dSOI change events and no severe weather occurrences. Here we calculate forecast success or probability of detection, false alarm rate, critical success, and these expressions are given as

$$\text{POD} = X(X+Y)^{-1}, \quad (3)$$

$$\text{FAR} = Z(X+Z)^{-1}, \quad (4)$$

$$\text{CSI} = X(X+Y+Z)^{-1}. \quad (5)$$

Additionally, the number of severe weather events associated with dSOI changes due to random chance (HC) (SWPC, 2021) were estimated since there was a high FAR, and this is calculated as

$$\text{HC} = (X+Y)(X+Z) \text{ number of days}^{-1}. \quad (6)$$

This quantity was used as one measure of the value of using the dSOI changes to identify severe weather events. The value will be a decimal number greater than zero. However, in order to make HC consistent with POD, FAR, and CSI, or a number between 0 and 1, we divide by the number of correct forecasts (X) and present this as the ratio of random hits to hits. Also, if the majority of severe weather events associated with dSOI changes were forecast as random hits, then dSOI is not a useful indicator for the future occurrence of severe weather events. The HC index could then be used in conjunction with the CSI index to calculate the Gilbert Skill Score (GSS) (SWPC, 2021) which is

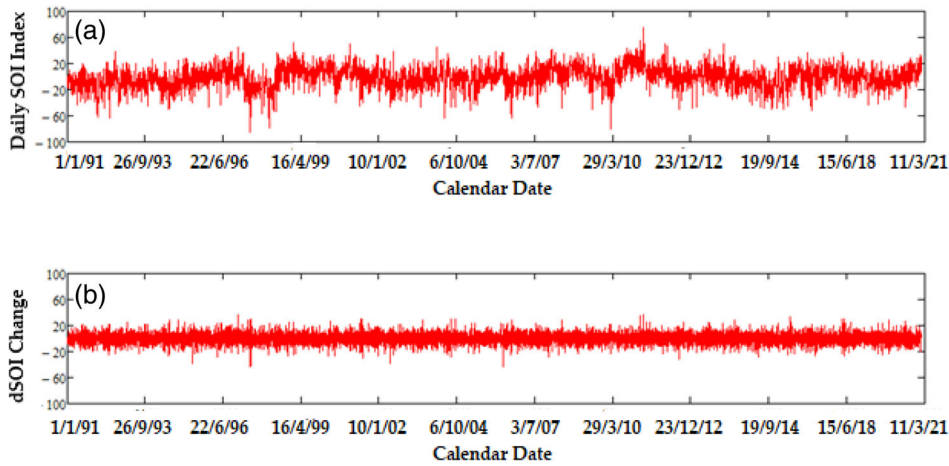


FIGURE 1 The (a) observed daily SOI (dSOI) and (b) 24-hr dSOI change for the study period. The abscissa is the calendar date (dd/mm/yy) and the ordinate is (a) dSOI and (b) 24-hr dSOI change. Data available through the Bureau of Meteorology (BOM) (Australia) website (<https://data.longpaddock.qld.gov.au/SeasonalClimateOutlook/SouthernOscillationIndex/SOIDataFiles/DailySOI1887-1989Base.txt>) [Colour figure can be viewed at wileyonlinelibrary.com]

$$GSS = (X - HC) (X + Y + Z - HC)^{-1}. \quad (7)$$

As a measure of skill, the GSS will be a value between 0 and 1, reflecting the value of a certain forecast above a certain baseline (e.g., Renken *et al.*, 2017; Klaus *et al.*, 2020), in this case a random hit. A score of zero would represent a useless forecast, while a score of unity would represent a perfect forecast.

3 | DAILY SOI INDEX VARIABILITY

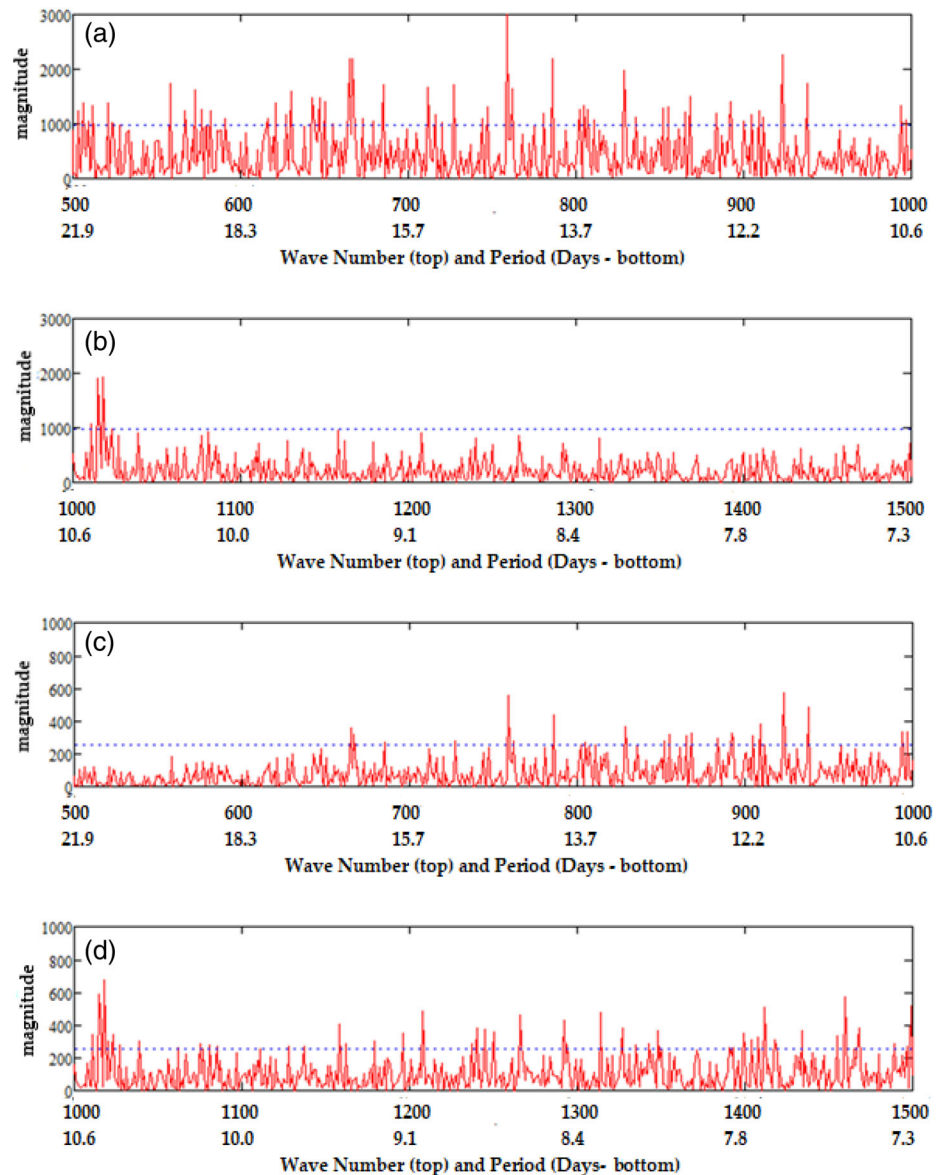
3.1 | Time series

The dSOI index values and the daily change in dSOI were analysed here in order to determine if short-term variability in this index can be identified. Typically, this index is analysed monthly in order to determine the current phase of ENSO. Lupo *et al.* (2014), Newberry *et al.* (2016), and Henson *et al.* (2017) all use the change in phase of ENSO over the Northern Hemisphere summer season to differentiate the dominant weather and climate regimes and these depended on the direction of the ENSO phase transition. Jensen and Lupo (2013) showed the correspondence of the time rate of change in the daily integrated enstrophy (IE) across the Northern Hemisphere along with local maxima of IE could be associated with blocking onset and termination, and later Jensen *et al.* (2018) and Klaus *et al.* (2020) showed that these quantities could be associated with large-scale (hemispheric) flow regime transitions. Gensini and Marinaro (2016) used the global relative atmospheric angular momentum and the time derivative to correlate with the occurrence of tornado outbreaks. Thus, there is precedent for examining teleconnection indices and their time rate of change.

Figures 1 and 2 show the dSOI and daily dSOI change from 1991 to 2020 in Cartesian space (Figure 1) and the Fourier transform of this time series which is in wave space (Figure 2). In Figure 1, the mean dSOI and mean daily dSOI change was -1.3 and 0.0 units, respectively, and the standard deviations were 15.6 and 8.0 units, respectively. In section 4.2, a daily dSOI change of 10 units and 3-day change of 20 units will be used to detect severe weather events since these values are larger than one standard deviation of the dSOI change.

In Figure 2, wave numbers 500–1,500 are shown for the dSOI and dSOI change time series, which correspond to waves with a period of 7–20 days. The blue dashed line shows the $p = .05$ confidence level using a white noise spectrum (Wilks, 2006). If the full spectrum were shown, the dSOI displays the greatest power at much longer periods (low wave number), while the daily change in dSOI displays the greatest power at shorter periods (high wave number). Significant periods shown near wave number 670, 760, and 780 correspond to 16, 15, and 14 days (Figure 2a), respectively. Other peaks in the dSOI are evident near wave number 560, 920, 940, 1,020, and 1,160 (Figure 2a,b) which correspond to 20, 12, 11, and 10 days, respectively. There are two peaks (140 and 210) are not shown here but they are consistent with the MJO period (e.g., Thompson and Roundy, 2013). There are two other peaks (360—not shown and 560—30 and 24 days, respectively) which are consistent with results shown in Branstator (1987) or Renken *et al.* (2017) for mid-latitude flows. The latter four periods (920, 940, 1,020, and 1,160, or 10–12 days) are similar to those associated with mid-latitude large-scale weather regimes (e.g., see Jensen *et al.*, 2018). In Figure 2c, the same 14–16-day periods in the dSOI change are evident and correspond to the same periods in the dSOI index (Figure 2a). There are peaks in the daily change in the SOI index from wave numbers 900–1,470 corresponding with periodicities of 7–12 days. These results mirror the

FIGURE 2 The (a, b) dSOI index and (c, d) daily (24 hr) change in dSOI index in wave space for wave numbers (a, c) 500–1,000, and (b, d) 1,000–1,500. The blue dashed line shows the $p = .05$ confidence level using a white noise spectrum (Wilks, 2006). The abscissa is wave number (top) and period (days; bottom) and the ordinate is spectral power [Colour figure can be viewed at wileyonlinelibrary.com]



results of Renken *et al.* (2017) who show the 8–12-day periodicities in the daily Pacific North American (PNA) Index. Also, in section 4, these periods will be used for the detection of severe weather experiment.

3.2 | Daily SOI events climatology

The monthly distributions were also examined (Figure 3), and the number of 10-point dSOI charges peaked in May, August, and November regardless of the ENSO year. This resulted in the NH spring (Southern Hemisphere fall) being the season with the largest number of these changes. The number of 20-point change events per month was comparable in terms of which months showed the strongest peaks. These distributions were all the same using the chi-square goodness-of-fit test at $p = .01$. The strong spring

peak and lesser NH fall peaks are also likely due to the annual cycle in SPCZ activity, which is most active in the austral summer and into the fall (e.g., Vincent, 1994; Folland *et al.*, 2002), as well as the mid-latitude jet stream, cyclone activity, and blocking (e.g., Wiedenmann *et al.*, 2002, and references therein).

4 | RELATIONSHIP TO SEVERE WEATHER

4.1 | Major severe weather events

In order to examine the relationship of the dSOI changes to major severe weather days, severe weather days were identified using the criterion described in section 2. The temporal distribution of these major events is shown in

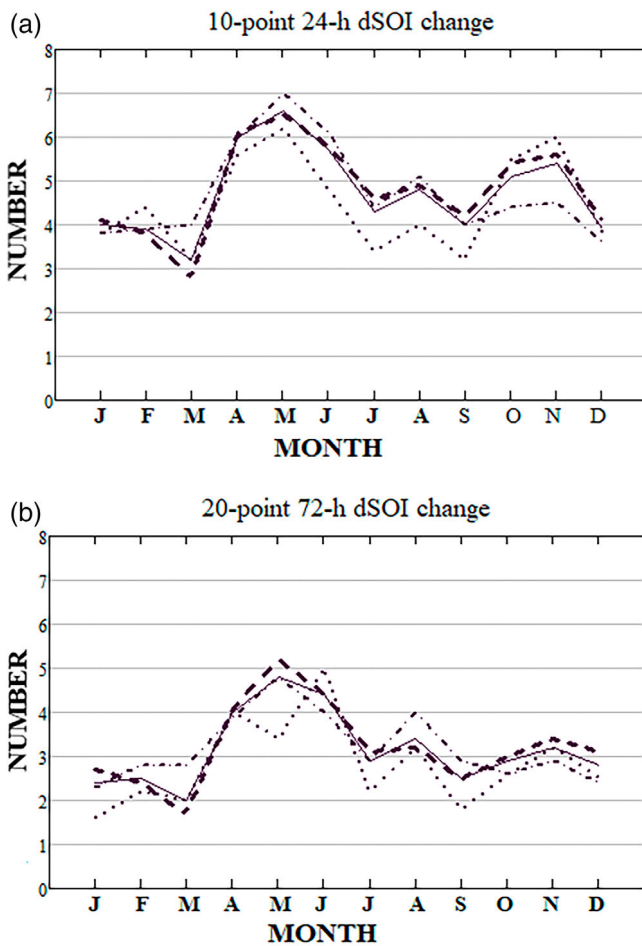


FIGURE 3 The number of (a) 10-point 24-hr and (b) 20-point 72-hr dSOI change events per month as separated by phase of ENSO. The ordinate is the number of events and the abscissa is the calendar month. The thin solid, dotted, dot-dash, thick dash lines represent the number of events per year for the total (1991 – 2020), LN, EN, and NEU years, respectively.

Figure 4 as stratified by phase of ENSO. For days with 20 or more tornado reports (Figure 4a), the peak occurrence for LN (4 of 6 years) and Neutral (6 of 17 years) (NEU) years is in April. For LN years, the peak season was March–May which is the earliest season, while for NEU years the peak season was April–July. For EN years, the peak month was May (3 of 7 years), while the peak season was March–June. EN and LN years showed similar annual occurrences (about 13 days), while NEU years had a mean occurrence of 10.8 days.

An examination of the annual variation of the peak occurrence for significant tornado days was performed by averaging the number corresponding to the calendar month(s) associated with a particular year's peak occurrence. This verified the April peak overall (4.8) and the standard deviation was 1.4 months. Most years observed the peak occurrence in April or May (24 years). If the peak

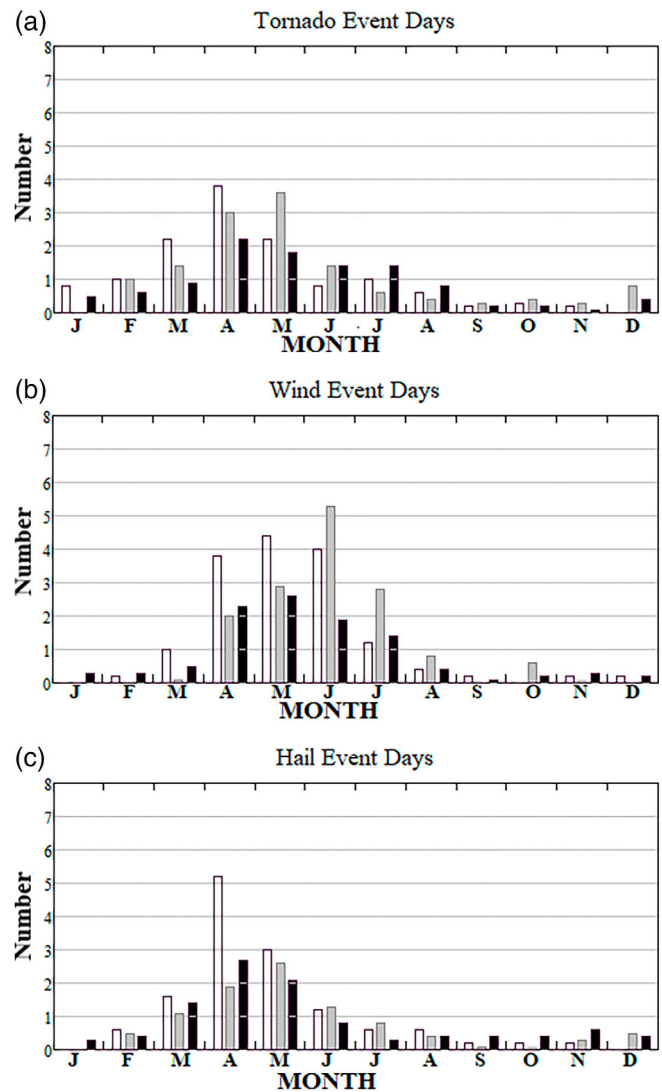


FIGURE 4 The mean monthly occurrence of days with; (a) 20 or more tornado reports, (b) 155 or more wind event reports (speeds $\geq 25.9 \text{ m}\cdot\text{s}^{-1}$), and (c) 135 or more hail (diameter $\geq 25.4 \text{ mm}$) reports. The ordinate is a mean monthly number of days and the abscissa is the month of the year. The unfilled, grey, and black bars represent La Nina, El Niño, and Neutral Years, respectively.

occurrence was in multiple months (e.g., April and May), the peak was presented as an average of these months (4.5). For only 1 year (July 2010) did the peak occurrence happen outside the first half of the year. However, caution must be taken when analysing the peak month of occurrence in this manner since not all peak months have a similar number of significant tornado days.

For wind event days (Figure 4b), the annual distributions were similar at $p = .01$ as well. The mean annual number of major severe days were similar for LN and EN years (15 vs. 14, respectively), while NEU years showed fewer occurrences (10.2 days), and this result is

significant at $p = .05$. The peak season for wind event days was later than that for tornadoes in general as shown in previous studies, and May was the peak month (mean of the total sample = 5.3) of occurrence. The maximum was observed in May for 14 years and June for 9 years, and the standard deviation was the smallest for major severe wind days (1 month). During LN and NEU years the peak season was April–June with an absolute maximum in May. May was the peak month for four of six LN and nine of 17 NEU years. For EN years, the season was April–July with a peak in June, and 4 of 7 years showed the peak in June or July.

For major hail event days (Figure 4c), the annual mean number of days was larger for LN years (13 days) when compared to EL and NEU years (9.5 and 10 days, respectively) and this difference is significant at $p = .05$. The annual distributions are all similar at $p = .01$. The seasonal distribution is similar for LN (3 of 6 years) and NEU (9 of 17 years) years shows an absolute peak in April (mean total sample = 4.7), while EN years peaked in May (5 of 7 years). The severe weather season is earliest for this variable beginning in March for every ENSO phase but terminating in May for EN years and June for LN and NEU years. Major hail event days also showed the largest variation as measured by standard deviation (1.7 months).

The temporal distribution of severe weather event findings are similar to several previous publications in spite of a different criterion chosen for what constitutes a major severe weather day (e.g., Cook and Schaefer, 2008; Cook *et al.*, 2017) and these found that the number of tornado days did not show strong interannual variability. The Cook *et al.*'s (2017) study covered a longer period of record and counted all tornado days. However, it is apparent in this study that NEU years show fewer major tornado day occurrences than either LN or LN years. The same was found for wind event days. Since this study examined severe weather reports over the CONUS, the above analysis alone cannot answer the question of whether there is spatial variability in major severe weather days with respect to ENSO.

4.2 | Using daily SOI and the daily change to detect severe weather days

An examination of the mean daily change in the dSOI (dSOI itself) was calculated to be close to zero (-1.5 units-day⁻¹) and the standard deviation was 8 (15.7) units. Thus, a change of 10 dSOI units-day⁻¹ is larger than one standard deviation, while a 20-point change over 3 days is greater than two standard deviations. During the 30-year period, there were 1,708 and

TABLE 3 The number of event days with 20 or more tornado reports associated with (a) 10-point 24-hr and (b) 20-point 72-hr changes in the dSOI by ENSO phase at 9–11 calendar days and 19–21 calendar days before outbreak and the fraction of the total days (POD)

	LN	EN	NEU	Total
10-point 24-hr change				
9–11 days	28/0.43	43/0.42	88/0.46	159/0.44
19–21 days	19/0.29	45/0.44	80/0.42	144/0.40
No dSOI change	22	29	47	98
Total w/o overlap	43/0.66	74/0.72	143/0.75	260/0.73
20-point 72-hr change				
9–11 days	31/0.48	45/0.44	87/0.46	163/0.46
19–21 days	20/0.31	38/0.37	76/0.40	134/0.37
No dSOI change	22	39	62	123
Total w/o overlap	43/0.66	64/0.62	128/0.67	235/0.66
Total outbreaks	65	103	190	358

Note: The total number of outbreaks identified excludes the event days identified by both periods.

1,129 dSOI 10-point daily (24 hr) change and 20-point 3-day change (72 hr) events, respectively. Often, these events occurred in succession or in episodes.

Large changes in the dSOI are lagged from one to 30 days prior to just one or more severe weather reports for each mode of severe weather and examined (Table 2) for April through June, it is apparent that there is little difference in the mean number severe weather reports corresponding to these lags. However, when testing these means versus the dSOI lag for significance using a t test (Table 2), there is a preference for the occurrence of severe weather lagged at approximately 16 days. This corresponds to significant dSOI and dSOI change variability identified in Figures 1 and 2. What is not clear is whether the result in Table 2 is associated with a singular physical phenomenon (e.g., cycles associated with global angular momentum; Gensini and Marinaro, 2016), if this represents constructive interference between short period fluctuations (e.g., vascillation; Jensen *et al.*, 2018, and references therein) and the longer period Rossby wave action identified by Renken *et al.* (2017) and several others, or was due to chance occurrence.

As shown in section 3, there are periodicities in the dSOI and the daily change of dSOI between approximately 8 and 12 days, as well as at 16 and 24 days. These periodicities are similar to those found in previous research cited earlier and the results in section 3. Thus, in order to test whether these large changes in dSOI correlate to major severe weather days, statistics such as the POD, FAR, and CSI were determined by examining the

TABLE 4 As in Table 3, but for 155 or more wind event (speeds $\geq 25.9 \text{ m}\cdot\text{s}^{-1}$) reports

	LN	EN	NEU	Total
10-point 24-hr change				
9–11 days	44/0.58	55/0.50	92/0.51	191/0.52
19–21 days	28/0.37	57/0.52	82/0.46	167/0.46
No dSOI change	23	27	50	100
Total w/o overlap	53/0.70	83/0.75	129/0.72	265/0.73
20-point 72-hr change				
9–11 days	40/0.53	57/0.52	85/0.47	182/0.50
19–21 days	28/0.37	49/0.45	82/0.46	159/0.44
No dSOI change	23	33	51	107
Total w/o overlap	53/0.70	77/0.70	128/0.71	258/0.71
Total outbreaks	76	110	179	365

TABLE 5 As in Table 3, except for days with 135 or more hail (diameter $\geq 25.4 \text{ mm}$) reports

	LN	EN	NEU	Total
10-point 24-hr change				
9–11 days	27/0.41	42/0.56	77/0.46	146/0.47
19–21 days	25/0.38	35/0.44	81/0.48	141/0.46
No dSOI change	25	17	40	82
Total w/o overlap	41/0.62	58/0.77	128/0.76	227/0.73
20-point 72-hr change				
9–11 days	35/0.53	31/0.41	74/0.44	140/0.45
19–21 days	25/0.38	38/0.51	78/0.46	141/0.46
No dSOI change	18	21	52	91
Total w/o overlap	48/0.73	54/0.72	116/0.69	218/0.71
Total outbreaks	66	75	168	309

daily changes in the dSOI index with a lag of 9–11 and 19–21 calendar day period previous to the major severe weather day (Tables 3–6) for all days of the year. These intervals were chosen since they are at the mid-points of the periodicities described above and provide for a more rigorous test of the POD. The number of missed forecasts was also counted. A miss is determined to be an event that was not preceded by a large dSOI change in either the 10-point 24-hr change or the 20-point 72-hr change.

There were 358 event days in which 20 or more tornadoes were reported. Table 3 demonstrated that 159 and 144 of these events were preceded by a 10-point 24-hr change in the dSOI index 9–11 and 19–21 calendar days before the event, respectively. For 20-point changes over 72-hr, these numbers were 163 and 134 days, respectively. Separately, this represents about 37–44% of all severe weather events being preceded by large changes in

dSOI at 7–11 days or 19–21 days prior (Table 3). For the total number of events identified in Table 3, those that were preceded by changes in both time periods (*and condition*) were counted only once. Thus, 73% of events were preceded by strong changes in the dSOI index in either range (9–11 and 19–21 calendar days) for a 24-hr dSOI change of 10 points, and 66% for a 72-hr change of 20 points in dSOI. This means only 27 and 34% of these events, respectively, were counted as a miss. This is fewer misses than either the 9–11 or 19–21 calendar day categories separately.

Examining these events by phase of ENSO (Table 3) annually demonstrates that there is no significant variability in the percentage of major tornado days preceded by 10-point 24-hr dSOI change or a 20-point 72-hr dSOI change at 9–11 calendar days before the event. However, 19–21 calendar days beforehand, 10-point 24-hr dSOI changes or 20-point 72-hr dSOI changes are more likely to be associated with severe weather in EN and NEU years. Thus, if both categories are considered, EN and NEU years are associated with the larger POD than LN years.

The annual results for wind event (Table 4) and hail event (Table 5) days are similar for the 10-point 24-hr changes in dSOI to the major tornado day results. Both Tables 4 and 5 showed a 73% POD overall, and for wind event days the POD is larger for EN years versus NEU and LN years. The POD for hail event days is lowest for LN years.

As noted above, the test performed here is more rigorous in order to demonstrate the value of large daily changes in dSOI indicating the possibility of severe weather 9–11 or 19–21 calendar days later. The periodicities identified in the dSOI and change in dSOI time series (Figure 2) is likely to vary by season and ENSO phase as discussed in Renken *et al.* (2017). If the test interval used here was wider, or varied according to season or ENSO phase, a much higher POD would have been identified. In the case of a test with a wider interval, the POD would have been overestimated arguably.

Nonetheless, since most severe weather days occur in the April–June time frame (Figure 4) (191 of 358 major tornado, 258 of 365 major wind, and 187 of 308 major hail day events) and certainly in the February–July time frame, the outcome here suggests that a large change in the dSOI index during these months may be a signal to a forecaster to anticipate the possibility of severe weather in the United States 1–3 weeks prior to its actual occurrence. A similar result was found recently by Gensini and Marinaro (2016) who used global atmospheric angular momentum time series and the change with time or Miller *et al.* (2020) who used a statistical-dynamic model of weather regimes to demonstrate skill in anticipating

TABLE 6 Signal detection and skill score statistics for severe weather modes and dSOI changes presented in Tables 3–5 for all LN, EL, and NEU years

		All	LN	EL	NEU
Tornado event days	POD	0.726/0.656	0.662/0.662	0.718/0.621	0.753/0.674
	FAR	0.848/0.793	0.849/0.758	0.839/0.791	0.852/0.803
	CSI	0.144/0.187	0.131/0.215	0.152/0.186	0.141/0.180
	HC	0.215/0.157	0.224/0.140	0.218/0.168	0.201/0.158
	GSS	0.116/0.162	0.104/0.191	0.122/0.159	0.115/0.156
Wind event days	POD	0.726/0.707	0.697/0.697	0.775/0.700	0.721/0.715
	FAR	0.845/0.772	0.814/0.702	0.819/0.748	0.867/0.803
	CSI	0.146/0.208	0.172/0.263	0.171/0.227	0.127/0.183
	HC	0.215/0.146	0.213/0.133	0.208/0.150	0.219/0.148
	GSS	0.119/0.183	0.141/0.237	0.140/0.200	0.102/0.160
Hail event days	POD	0.735/0.706	0.621/0.727	0.773/0.720	0.762/0.690
	FAR	0.867/0.808	0.856/0.730	0.874/0.824	0.868/0.821
	CSI	0.127/0.178	0.133/0.245	0.122/0.165	0.127/0.165
	HC	0.213/0.147	0.239/0.208	0.203/0.145	0.207/0.154
	GSS	0.102/0.156	0.104/0.204	0.100/0.145	0.103/0.144

Note: These are presented as 10-point 24-hr/20-point 72-hr dSOI change events. The HC is shown as the ratio of random hits to hits.

tornado outbreak days 1–3 weeks prior to the event. These investigations examined only tornado days while this work included other severe convective weather phenomena such as hail and wind events. Additionally, this outcome is similar to the forecast value found by Renken *et al.* (2017) to anticipate extreme weather 1–3 weeks in advance using the BSR or EAR indices.

As expected, the FAR was higher than the POD (Table 6) for the annual occurrence of tornado days with more than 20 reports, but this quantity was actually lower for the 20-point 72-hr dSOI change events. In spite of the high FAR, fewer than one in four and one in six forecast successes were considered to be the result of random chance (HC) for 10- and 20-point dSOI change events, respectively. These results above provided for CSI and GSS scores that were also higher for the 20-point dSOI change events. It is noted here that the GSS scores in Table 6 were on the order of 0.10–0.20, which means there is skill in the dSOI over random chance in the detection of major tornado days. If the skill score is a measure of value added to the forecast, the GSS here are higher than the value added by a human forecaster over 24-hr model forecasts which were 0.00–0.10 (see Lupo and Market, 2002). The scores here are also similar to the skill of using teleconnections in Renken *et al.* (2017) to forecast anomalous temperatures on the sub-seasonal scale, and about as high as winter season forecasts (two seasons ahead) for the central United States (see Lupo *et al.*, 2008).

If other measures of success are examined (HC, CSI, and GSS; see Table 6), the lowest (highest for HC) skill

values are found for 10-point 24-hr dSOI change LN events, while the highest (lowest for HC) skill values are associated with 20-point 72-hr SOI change LN events. However, in examining the measures of success in Table 6, the 20-point 72-hr dSOI change events showed the highest CSI and GSS for both wind event and hail event days as for tornado event days. For 10-point 24-hr dSOI change events, the HC rate is highest during LN years.

In order to make comparisons to the annual statistics, the same measures of forecast success examined above in Tables 3–6 were done for the peak/spring season only (March–May) for tornadoes, and hail (Figure 4a,c). These months accounted for more than one half of each sample, 192 event for tornadoes and 197 events for hail, For the wind events, April–June was examined and these months accounted for 257 of the 365 total events (Figure 4b). However, in spite of the fact that these months showed a peak in occurrence of dSOI change events, the number of these were only about 30% of the annual number of events. These results are presented in Table 7.

Examining the dSOI change detection statistics for only the peak time of year for both dSOI and major severe weather days showed improvement in the POD of severe weather for 10-point 24-hr dSOI change events (Table 7). As shown earlier, the peak time of year for both are similar. The FAR decreased substantially and in many cases were less than the POD. The CSI and GSS were improved substantially as well. The improvement in

TABLE 7 As in Table 6, except for the peak months of occurrence only

		All	LN	EL	NEU
Tornado event days, Mar–May	POD	0.720/0.370	0.630/0.150	0.750/0.440	0.740/0.410
	FAR	0.708/0.785	0.667/0.872	0.647/0.692	0.752/0.809
	CSI	0.262/0.156	0.278/0.074	0.316/0.220	0.229/0.150
	HC	0.238/0.324	0.261/0.682	0.246/0.283	0.227/0.294
	GSS	0.212/0.111	0.222/0.025	0.258/0.169	0.186/0.111
Wind event days, Apr–Jun	POD	0.760/0.410	0.767/0.480	0.770/0.290	0.740/0.460
	FAR	0.647/0.733	0.446/0.524	0.588/0.765	0.728/0.774
	CSI	0.317/0.193	0.474/0.315	0.366/0.150	0.248/0.179
	HC	0.266/0.355	0.238/0.277	0.273/0.479	0.274/0.328
	GSS	0.254/0.134	0.407/0.250	0.296/0.084	0.193/0.128
Hail event days, Mar–May	POD	0.730/0.370	0.740/0.240	0.820/0.430	0.690/0.400
	FAR	0.696/0.776	0.520/0.745	0.735/0.791	0.725/0.777
	CSI	0.274/0.162	0.409/0.143	0.250/0.164	0.245/0.168
	HC	0.234/0.319	0.222/0.417	0.222/0.286	0.242/0.298
	GSS	0.224/0.117	0.350/0.089	0.205/0.123	0.197/0.124

GSS values to 0.19–0.41 means that the skill for the peak season of occurrence especially at the high end of the range were nearly as high as short range dynamic model 500 hPa height forecasts at the 7–10 calendar day range (Klaus *et al.*, 2020). For CSI, these values were generally lower than 0.20 in Table 6, but generally higher than 0.25 to as much as 0.47 in Table 7. The CSI values in Table 7 were higher than those found for tropical cyclone intensity found by Tam *et al.* (2021) which ranged between 0.2–0.3. The ratio of random hits was also slightly higher, but not substantially. For the 20-point 72-hr dSOI changes during the peak time of the year, the measures of forecast skill such as POD were decreased, and the estimated number of random hits was higher. Measures such as FAR, CSI, and GCC were similar to the overall, but in some cases (e.g., LN year tornado and hail event days) were substantially worse than the annual results overall. In order to investigate this association more closely, the next step in this work may be to isolate active synoptic-scale weather patterns and determine if a similar improvement can be found in the POD of severe weather for significant changes in the dSOI regardless of time of year.

In Tables 6 and 7, the high FAR are of particular concern. For the entire year the FAR are higher than the POD (Table 6) and generally between 0.73 and 0.87. When the study samples are limited to the 3 months of the year when the occurrence of severe weather is higher (Table 7), and the number of 10-point 24-hr dSOI changes is marginally higher, the POD is generally higher than the FAR, which is generally between 0.45 and 0.81.

A cursory examination of the published literature shows many studies of FAR (e.g., Barnes *et al.*, 2007) address the issue of human forecasts, model forecasts, or warnings corresponding to the occurrence of dangerous phenomenon such as severe weather. Fewer (e.g., Renken *et al.*, 2017) calculate FAR using a predictor variable which precedes a target (or predictand) variable. In Renken *et al.* (2017) the FAR was on the order of 0.29–0.35 when comparing teleconnection indices to significant (2σ) temperature outbreaks in the central United States.

The reasons for the high FAR found here are not immediately clear, and more study would need to be done to determine why this problem exists. Several variables could be examined including the magnitude of the dSOI change criterion, the “forecast” lead time interval, or what constitutes a major severe weather day. The criterion for a severe weather day was chosen subjectively here in order to provide a large sample for study. The former two variables would change what constitutes a successful forecast (POD) as well as the FAR. Another issue may be the narrow verification intervals for severe weather and the dSOI as identified earlier. In combination with the limits of dynamic predictability for synoptic-scale weather phenomenon, including those that are responsible for severe weather events, is at the edge of the 9–11-day POD interval also may partly contribute to the higher FAR rates. Nonetheless, in spite of the higher FAR, the discussion above demonstrated that the measures of success when using dSOI change to anticipate the occurrence of severe weather in the USA were comparable to those found in other studies.

5 | SUMMARY AND CONCLUSIONS

This work examined the occurrence of major severe weather days defined as 20 or more tornado, 155 or more wind reports (speeds $\geq 25.9 \text{ m}\cdot\text{s}^{-1}$), and 135 or more hail reports (diameter $\geq 25.4 \text{ mm}$) and then related this to periodicity found in the time series of the dSOI and the change with time of this index. The time period studied was the most recent 30 years (1991–2020). Using data provided by the NCEP/NCAR reanalyses and the severe weather archives found at the SPC in Norman, OK, the following results were obtained:

- There were significant periodicities found in the time series of dSOI and the change with time of this index, and these are similar to the results found in many other studies when analysing teleconnection index time series.
- There were more major severe weather days from January to April found in LN years and then from June to August there were more major severe weather days toward the end of the EN phase (since the phase transition occurs in the Northern Hemisphere fall). Here we found that most major severe weather days occurred during April and May. These results are similar to Cook *et al.* (2017) who studied only tornado days in the early part of the year, for a longer time period.
- There was a lag of approximately 16 days found between the time of a major change in the SOI index and the occurrence of any severe weather in the United States when counting the days when at least one severe weather event occurred.
- There was a POD on the order of 70% for major severe weather days when a 10-point 24-hr change in the dSOI or a 20-point 72-hr change in the dSOI occurred 1–3 weeks previously when tested using a relatively narrow band for this lag. This result is for the entire year. The results found here likely underestimated the POD but suggests utility in anticipating severe weather 1–3 weeks in advance using a teleconnection index such as the dSOI. This result corroborates those of Miller *et al.* (2020) who used different techniques. However, the FAR was higher than the POD.
- The number of dSOI change events varied annually as well showing a peak in the Northern Hemisphere spring season, which corresponds to the peak time for severe weather occurrence. The number of dSOI change events were smallest in LN years.
- With respect to ENSO, these severe weather events were preceded by 10-point 24-hr changes dSOI most often in EN years and the POD was about 10 percentage points less in LN years. There was no ENSO variability in the 20-point 72-hr changes in dSOI.
- When testing the performance metrics during the peak severe weather season, there was improvement for the 10-day 24-hr dSOI change events corresponding to severe weather events. But, the 20-point 72-hr dSOI changes over 3 days showed somewhat degraded skill. During the peak severe weather season, the POD was higher than the FAR, and more investigation would be needed to determine why the FAR is relatively large in this work.

ACKNOWLEDGEMENTS

The authors acknowledge the time and effort of the two anonymous reviewers, whose time and effort helped to make this work stronger.

CONFLICT OF INTEREST

The authors declare no potential conflict of interest.

ORCID

Anthony R. Lupo  <https://orcid.org/0000-0002-5810-5652>

REFERENCES

- Akyuz, F.A., Chambers, M.D. and Lupo, A.R. (2004) The short and long-term variability of F2 or stronger (significant) tornadoes in the central plains. *Transactions of the Missouri Academy of Science*, 38, 26–45.
- Allen, J., Tippett, M. and Sobel, A. (2015) Influence of the El Niño/Southern Oscillation on tornado and hail frequency in the United States. *Nature Geoscience*, 8, 278–283. <https://doi.org/10.1038/ngeo2385>.
- Baggett, C.F., Nardi, K.M., Childs, S.J., Zito, S.N., Barnes, E.A. and Maloney, E.D. (2018) Skillful subseasonal forecasts of weekly tornado and hail activity using the Madden–Julian Oscillation. *Journal of Geophysical Research: Atmospheres*, 123, 12661–12675. <https://doi.org/10.1029/2018JD029059>.
- Barnes, L.R., Grunfest, E.C., Hayden, M.H., Schultz, D.M. and Benight, C. (2007) False alarms and close calls: a conceptual model of warning accuracy. *Weather Forecasting*, 22, 1140–1147.
- Barrett, B.S. and Gensini, V.A. (2013) Variability of central United States April–May tornado day likelihood by phase of the Madden–Julian Oscillation. *Geophysical Research Letters*, 40, 2790–2795.
- Barrett, B.S. and Henley, B.N. (2015) Intraseasonal variability of hail in the contiguous United States: relationship to the Madden–Julian Oscillation. *Monthly Weather Review*, 143, 1086–1103.
- Bjerknes, J. (1966) A possible response of the atmospheric Hadley circulation to equatorial anomalies of ocean temperature. *Tellus*, 18(4), 820–829.
- Bjerknes, J. (1969) Atmospheric teleconnections from the equatorial Pacific. *Monthly Weather Review*, 97(3), 163–172.
- Bosart, L.F., Moore, B.J., Cordeira, J.M. and Archambault, H.M. (2017) Interactions of North Pacific tropical, midlatitude, and polar disturbances resulting in linked extreme weather events over North America in October 2007. *Monthly Weather Review*, 145, 1245–1273. <https://doi.org/10.1175/MWR-D-16-0230.1>.
- Branstator, G. (1987) A striking example of the atmosphere's leading traveling pattern. *Journal of the Atmospheric Sciences*, 44,

- 2310–2323. [https://doi.org/10.1175/1520-0469\(1987\)044<2310:ASEOTA>2.0.CO;2](https://doi.org/10.1175/1520-0469(1987)044<2310:ASEOTA>2.0.CO;2).
- Brooks, H.E. (2004) Tornado—warning performance in the past and future: a perspective from signal detection theory. *Bulletin of the American Meteorological Society*, 85, 837–844.
- Cook, A.R., Leslie, L.M. and Parsons, D.B. (2017) The impact of El Niño–Southern Oscillation (ENSO) on winter and early spring U.S. tornado outbreaks. *Journal of Applied Meteorology and Climatology*, 56, 2455–2478.
- Cook, A.R. and Schaefer, J.T. (2008) The relation of El Niño–Southern Oscillation (ENSO) to winter tornado activity. *Monthly Weather Review*, 136(8), 3121–3137.
- Dixon, P.G., Mercer, A.E., Choi, J. and Allen, J.S. (2011) Tornado risk analysis: Is Dixie Alley an extension of Tornado Alley? *Bulletin of the American Meteorological Society*, 92, 433–441.
- Farrar, J.T. (2011) Barotropic Rossby waves radiating from tropical instability waves in the Pacific Ocean. *Journal of Physical Oceanography*, 41, 1160–1181. <https://doi.org/10.1175/2011JPO4547.1>.
- Folland, C.K., Renwick, J.E., Salinger, M.J. and Mullan, A.B. (2002) Relative influences of the Interdecadal Pacific Oscillation and ENSO in the South Pacific Convergence Zone. *Geophysical Research Letters*, 29(13), 1643. <https://doi.org/10.1029/2001GL014201>.
- Gensini, V.A. and Allen, J.T. (2018) U.S. hail frequency and the global wind oscillation. *Geophysical Research Letters*, 45, 1611–1620. <https://doi.org/10.1002/2017GL076822>.
- Gensini, V.A., Barrett, B.S., Allen, J.T., Gold, D. and Sirvatka, P. (2020) The extended-range tornado activity forecast (ERTAF) project. *Bulletin of the American Meteorological Society*, 101, E700–E709.
- Gensini, V.A., Gold, D., Allen, J.T. and Barrett, B.S. (2019) Extended U.S. tornado outbreak during late May 2019: a forecast of opportunity. *Geophysical Research Letters*, 46, 10150–10158. <https://doi.org/10.1029/2019GL084470>.
- Gensini, V.A. and Marinaro, A. (2016) Tornado frequency in the United States related to global relative angular momentum. *Monthly Weather Review*, 144, 801–810. <https://doi.org/10.1175/MWR-D-15-0289.1>.
- Gensini, V.A. and Tippet, M.K. (2019) Global ensemble forecast system (GEFS) predictions of days 1–15 U.S. tornado and hail frequencies. *Geophysical Research Letters*, 46, 2922–2930. <https://doi.org/10.1029/2018GL081724>.
- Gollan, G. and Greatbatch, R.J. (2017) The relationship between Northern Hemisphere winter blocking and tropical modes of variability. *Journal of Climate*, 30, 9321–9337.
- Henderson, S.A., Maloney, E.D. and Barnes, E.A. (2016) The influence of the Madden–Julian oscillation on Northern Hemisphere winter blocking. *Journal of Climate*, 29, 4597–4616.
- Henson, C.B., Lupo, A.R., Market, P.S. and Guinan, P.E. (2017) ENSO and PDO-related climate variability impacts on Midwestern United States crop yields. *International Journal of Biometeorology*, 61, 857–867. <https://doi.org/10.1007/s00484-016-1263-3>.
- Jensen, A., Lupo, A.R., Mokhov, I.I., Akperov, M.G. and Sun, F. (2018) The dynamic character of Northern Hemisphere flow regimes in a near term climate change projection. *Atmosphere*, 9(1), 27.
- Jensen, A.D. and Lupo, A.R. (2013) Using enstrophy advection as a diagnostic to identify blocking regime transition. *Quarterly Journal of the Royal Meteorological Society*, 139, 2–7. <https://doi.org/10.1002/qj.2248>.
- Kalnay, E., Kanamitsu, M., Kistler, R., Collins, W., Deaven, D., Gandin, L., Iredell, M., Saha, S., White, G., Woollen, J., Zhu, Y., Leetmaa, A., Reynolds, R., Chelliah, M., Ebisuzaki, W., Higgins, W., Janowiak, J., Mo, K.C., Ropelewski, C., Wang, J., Jenne, R. and Joseph, D. (1996) The NCEP/NCAR 40-year reanalysis project. *Bulletin of the American Meteorological Society*, 77, 437–471. [https://doi.org/10.1175/1520-0477\(1996\)077<0437:TNYRP>2.0.CO;2](https://doi.org/10.1175/1520-0477(1996)077<0437:TNYRP>2.0.CO;2).
- Klaus, E.M., Market, P.S., Lupo, A.R., Bodner, M.J. and Kastman, J. S. (2020) Projecting Northern Hemisphere flow regime transition using integrated enstrophy. *Atmosphere*, 11, 19.
- Lepore, C., Tippet, M.K. and Allen, J.T. (2017) ENSO-based probabilistic forecasts of March–May U.S. tornado and hail activity. *Geophysical Research Letters*, 44, 9093–9101. <https://doi.org/10.1002/2017GL074781>.
- Li, Y.C. (2018) Linear hydrodynamic stability. *Notices of The American Mathematical Society*, 65, 1255–1259.
- Lupo, A.R., Jensen, A.D., Mokhov, I.I., Timazhev, A.V., Eichler, T. and Efe, B. (2019) Changes in global blocking character during the most recent decades. *Atmosphere*, 10, 00092.
- Lupo, A.R., Kelsey, E.P., Weitlich, D.K., Davis, N.A. and Market, P. S. (2008) Using the monthly classification of global SSTs and 500 hPa height anomalies to predict temperature and precipitation regimes one to two seasons in advance for the mid-Mississippi region. *National Weather Digest*, 32(1), 11–33.
- Lupo, A.R. and Market, P.S. (2002) The verification of weather forecasts in Central Missouri and seasonal variations in forecast accuracy. *Weather Forecasting*, 8, 891–897.
- Lupo, A.R., Mokhov, I.I., Chende, Y.G., Lebedeva, M.G., Akperov, M. and Hubbard, J.A. (2014) Studying summer season drought in western Russia. *Advances in Meteorology*, 9, 942027.
- Marzban, C. and Schaefer, J.T. (2001) The correlation between U.S. tornadoes and Pacific Sea surface temperatures. *Monthly Weather Review*, 129, 884–895.
- Miller, D.E., Wang, Z., Trapp, R.J. and Harnos, D.S. (2020) Hybrid prediction of weekly tornado activity out to week 3: utilizing weather regimes. *Geophysical Research Letters*, 47, e2020GL087253. <https://doi.org/10.1029/2020GL087253>.
- Monfredo, W. (1999) Relationships between phases of the El Niño–Southern Oscillation and character of the tornado season in the south-central United States. *Physical Geography*, 20, 413–421.
- Moore, T.W. (2019) Seasonal frequency and spatial distribution of tornadoes in the United States and their relationship to the El Niño/Southern Oscillation. *Annals of the American Association of Geographers*, 109, 1033–1051.
- Moore, T.W. and McGuire, M.P. (2020) 2020: tornado-days in the United States by phase of the Madden–Julian Oscillation and Global Wind Oscillation. *Climate Dynamics*, 54, 17–36. <https://doi.org/10.1007/s00382-019-04983-y>.
- Moore, T.W., St. Clair, J.M. and DeBoer, T.A. (2018) An analysis of anomalous winter and spring tornado frequency by phase of the El Niño/Southern Oscillation, the Global Wind Oscillation, and the Madden–Julian Oscillation. *Advances in Meteorology*, 2018, 3612567. <https://doi.org/10.1155/2018/3612567>.
- Newberry, R.G., Lupo, A.R., Jensen, A.D. and Rodrigues-Zalipynis, R.A. (2016) An analysis of the spring-to-summer transition in the West Central Plains for application to long range forecasting. *Weather, Climate, and Society*, 6, 373–393.

- Nunes, M.J., Lupo, A.R., Lebedeva, M.G., Chendev, Y.G. and Solovyov, A.B. (2017) The occurrence of extreme monthly temperatures and precipitation in two global regions. *Papers in Applied Geography*, 3, 143–156. <https://doi.org/10.1080/23754931.2017.1286253>.
- Pan, L.-L. and Li, T. (2008) Interactions between the tropical ISO and midlatitude low-frequency flow. *Climate Dynamics*, 31, 375–388.
- Renken, J.D., Herman, J.J., Bradshaw, T.R., Market, P.S. and Lupo, A.R. (2017) The utility of the Bering Sea and East Asian rules in long range forecasting. *Advances in Meteorology*, 2017, 1765428. <https://doi.org/10.1155/2017/1765428>.
- Renwick, J.A. and Revell, M.J. (1999) Blocking over the South Pacific and Rossby wave propagation. *Monthly Weather Review*, 127, 2233–2247.
- Robertson, A.W., Kumar, A., Peña, M. and Vitart, F. (2015) Improving and promoting subseasonal to seasonal prediction. *Bulletin of the American Meteorological Society*, 96, ES49–EES53.
- Seo, K., Lee, H. and Frierson, D.M.W. (2016) Unraveling the teleconnection mechanisms that induce wintertime temperature anomalies over the Northern Hemisphere continents in response to the MJO. *Journal of the Atmospheric Sciences*, 73, 3557–3571. <https://doi.org/10.1175/JAS-D-16-0036.1>.
- Space Weather Prediction Center (SWPC). (2021) *Forecast verification glossary*. Available at: <https://www.swpc.noaa.gov/sites/default/files/images/u30/Forecast%20Verification%20Glossary.pdf>.
- Tam, H.-F., Choy, C.-W. and Wong, W.-K. (2021) Development of objective forecast guidance on tropical cyclone rapid intensity change. *Meteorological Applications*, 28, e1981. <https://doi.org/10.1002/met.1981>.
- Thompson, D.B. and Roundy, P.E. (2013) The relationship between the Madden–Julian Oscillation and violent tornado outbreaks in the spring. *Monthly Weather Review*, 141, 2087–2095.
- Tippett, M.K. (2018) Robustness of relations between the MJO and U.S. tornado occurrence. *Monthly Weather Review*, 146, 3873–3884.
- Vincent, D.G. (1994) The South Pacific Convergence Zone (SPCZ): a review. *Monthly Weather Review*, 122, 1949–1970.
- Wallace, J.M. and Gutzler, D.S. (1981) Teleconnections in the geopotential height field during the Northern Hemisphere winter. *Monthly Weather Review*, 109, 784–812.
- Wang, Y., Lupo, A.R. and Qin, J. (2013) A response in the ENSO cycle to an extratropical forcing mechanism during the El Niño to La Niña transition. *Tellus Series A*, 65, 22431.
- Weickmann, K. and Berry, E. (2009) The tropical Madden–Julian Oscillation and the Global Wind Oscillation. *Monthly Weather Review*, 137, 1601–1614. <https://doi.org/10.1175/2008MWR2686.1>.
- Wiedenmann, J.M., Lupo, A.R., Mokhov, I.I. and Tikhonova, E. (2002) The climatology of blocking anticyclones for the Northern and Southern Hemispheres: block intensity as a diagnostic. *Journal of Climate*, 15, 3459–3473.
- Wilks, D.S. (2006) *Statistical Methods in the Atmospheric Sciences*. *International Geophysics Series*, Vol. 91, 2nd edition. Cambridge, MA: Academic Press, p. 627.
- Zhao, P., Cao, C. and Chen, J. (2010) A summer teleconnection pattern over the extratropical Northern Hemisphere and associated mechanisms. *Climate Dynamics*, 35(2), 523–534.

How to cite this article: Renken, J. S., Brown, C. L., Kennedy, G., Mainguy, J., Wergelas, N., & Lupo, A. R. (2022). Using the daily change in the Southern Oscillation Index to develop analogues and the relationship to severe weather outbreaks. *International Journal of Climatology*, 1–15. <https://doi.org/10.1002/joc.7775>